Model for geometry optimisation of thermoelectric devices in a hybrid PV/TE system

H. Hashim [a, b], J.J. Bomphrey [a, 1], G. Min [a, *]

[a] Cardiff School of Engineering, Cardiff University, Cardiff, CF24 3AA, UK
[b] College of Engineering, Kerbala University, Kerbala, Iraq

ARTICLE INFO

ABSTRACT

A model for the geometry optimisation of thermoelectric devices in a hybrid photovoltaic - thermo-electric (PV/TE) system is presented. The model can be used to determine the optimal geometry of thermoelectric modules at which the maximum power output is achieved. The results of simulation using this model shows that an increase in both the overall power output and conversion efficiency may be achieved by incorporating a thermoelectric generator (TEG) to harvest waste heat from photovoltaic cell. In addition, the results demonstrate that the geometry optimisation also needs to consider the "trade-off" between achieving a large power output and minimising the consumption of thermoelectric materials.

© 2015 The Authors. Published by Elsevier Ltd. This is an open access article under the CC BY-NC-ND license (http://creativecommons.org/licenses/by-nc-nd/4.0/).

1. Introduction

A large proportion of solar energy is converted to waste heat in a photovoltaic (PV) cell, due to thermalisation of excited, high energy electrons and absorption of low energy photons, raising the temperature of the photovoltaic cell [1]. Therefore, there has been considerable interest in cooling PV cells using a number of cooling techniques [2–7], including the use of thermoelectric (TE) coolers. An alternative approach is to use the thermoelectric device as a generator to convert waste heat to electricity, [8–13]. The integration of different types of PV cells, such as dye sensitised solar cells, with thermoelectric generator (TEG) has been studied [14–17]. The results from these studies provide useful information on designing and improving the performance of the hybrid system. Recently, a hybrid system consisting of a polymer solar cell placed on the top of a TEG has been reported [18], in which the overall power generation of the hybrid PV/TE system has been investigated experimentally. The results indicate that the hybrid system is more efficient in generating electricity than using one system.

In a hybrid system, the dimension of the TEG has significant influence on the overall power output because it determines the operating temperature of the solar cell and the temperature difference across the TEG. To date, very few studies have focussed on geometry optimisation of the TEG to improve the performance of hybrid PV/TE system. The objective of this paper is to present a theoretical model that enables determination of optimal geometry of TEG to achieve maximum overall power output for a hybrid PV/TE system. A unique aspect of this model is that the temperature difference across the TEG is calculated under a closed-circuit condition, which provides more realistic calculation of the power output and efficiency than these obtained under open-circuit condition.

2. Model outline

A hybrid PV/TE system is shown schematically in Fig. 1. It consists of a PV cell on the top of a TEG via a copper plate that serves as a thermal concentrator. The interfaces are filled with thermally conductive paste to ensure good heat transfer across these interfaces. The copper plate forms the hot side of the TEG, with the cold side of the TEG attached to a heat exchanger with water circulating through it. The advantages of such a hybrid system are that the operating temperature of the PV cell will be reduced due to transfer the heat into the TEG and the TEG will generate additional power due to a temperature difference is established across it.

* Corresponding author.
E-mail address: min@cardiff.ac.uk (G. Min).
[1] Current address: Department of Chemistry, University of Warwick, Coventry, CV4 7AL, UK.
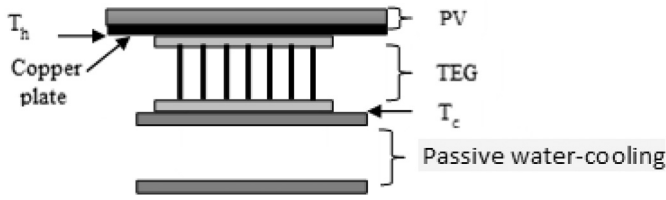
Fig. 1. A schematic diagram of photovoltaic and thermoelectric hybrid system.

In this hybrid system, the solar energy is converted to electrical energy and thermal energy. According to the law of conservation of energy, the energy balance of this system can be written as

$$\tau_g[\alpha_c\beta_c G + \alpha_T(1-\beta_c)G)]A_{PV} = Q_c + Q_r + Q_k + P_{PV} \quad (1)$$

where τ_g is the transmissivity of the glass cover, α_c is the absorptivity of the PV cell, β_c is the packing factor, G is the solar radiation intensity, α_T is the absorptivity of the tedlar and A_{PV} is the device area of the PV cell. On the right side of Eq. (1), Q_c denotes convective heat loss from the surface of the cell, Q_r is the radiative loss, Q_k is the heat conduction from the PV cell to TEG, and P_{PV} is the electrical power generated by the PV cell [19–21].

The heat loss due to convection and conduction from the PV cell to ambient is given by

$$Q_c = U_t A_{PV}(T_{cell} - T_{amb}) \quad (2)$$

where, T_{cell} and T_{amb} represent the solar cell and ambient temperatures, respectively. U_t is the heat transfer coefficient from the PV cell to the ambient by convection and conduction [22].

$$U_t = \left(\frac{L_g}{k_g} + \frac{1}{h_{cov}}\right)^{-1} \quad (3)$$

where, L_g and k_g are the thickness and thermal conductivity of the glass cover of the PV cell. h_{cov} is the convective heat transfer coefficient [23].

Radiative heat loss from the PV cell is described by

$$Q_r = \varepsilon\sigma A_{PV}\left(T_{cell}^4 - T_{amb}^4\right) \quad (4)$$

where, ε is the surface emissivity of the cell and σ is the Stefan–Boltzmann constant.

Heat conducted from the PV cell into TEG can be written as

$$Q_k = \frac{k \cdot A_{TE} \cdot N \cdot \Delta T}{l_{TE}} \quad (5)$$

where, k is the thermal conductivity of the thermoelectric material, A_{TE} is the cross-sectional area of thermoelements, N is the number of thermoelements and l_{TE} is the length of thermoelements. ΔT is the temperature difference across the TEG. It is assumed for simplicity that the effect of the solder and copper contacts has a negligible effect and consequently, ΔT can be approximated by $(T_{cell} - T_c)$ if the TEG operates in open-circuit (where, T_c is the temperature at the cold side of the TEG).

An important distinction is required here, as ΔT makes no reference to whether or not the TE device is in the open-circuit condition or the closed-circuit condition. In all previous studies, the power output of the TEG was calculated using a ΔT that corresponds to open-circuit condition. This can introduce significant error because the ΔT across a TEG at closed-circuit differs

significantly from that at open-circuit. In a real system, TEG has to operate in the closed-circuit condition in order to deliver the power to external load. Under such circumstances, the heat flow through the TEG consists of both heat conduction and the Peltier heat. As a result, the ΔT in Eq. (5) should be replaced by Refs. [24,25].

$$\Delta T = (1 + ZT_M)(T_{cell} - T_c) \quad (6)$$

where, Z ($= \alpha^2/\rho\cdot k$) is the thermoelectric figure of merit, α is the Seebeck coefficient, ρ is the electrical resistivity, T_M is given as

$$T_M = \frac{(1+2s)T_{cell} + T_c}{2(1+s)^2} \quad (7)$$

where, s is the ratio of the load resistance to the internal resistance of the TE module. Using Eq. (6) to replace ΔT in Eq. (5) with $s = 1$ (i.e., operating under the matched-load condition), we obtain

$$Q_k = \frac{k \cdot A_{TE} \cdot N \cdot \left[1 + \frac{Z(3T_{cell}+T_c)}{8}\right] \cdot (T_{cell} - T_c)}{l_{TE}} \quad (8)$$

The power output of the TEG, with taking into account the electrical and thermal contact resistances, can be expressed as [26].

$$P_{TE} = \frac{\alpha^2 \cdot A_{TE} \cdot N \cdot (T_{cell} - T_c)^2}{2 \cdot \rho \cdot (n + l_{TE}) \cdot \left(1 + \frac{2 \cdot r \cdot l_c}{l_{TE}}\right)^2} \quad (9)$$

where, l_c is the thickness of the ceramic plates of the TEG. The variables n and r are the electrical and thermal contact parameters, which correspond to the ratio of the bulk material electrical resistivity and thermal conductivity to that of the contacts, respectively [26].

From Eqs. (8) and (9), the conversion efficiency of the TEG, η_{TE}, can be calculated by

$$\eta_{TE} = \frac{P_{TE}}{Q_k} \quad (10)$$

The power output, P_{PV}, of the PV cell is given by

$$P_{PV} = \eta_{PV}\tau_g A_{PV}G \quad (11)$$

where, η_{PV} is the efficiency of the PV cell. It varies with temperature and can be expressed as [27].

$$\eta_{PV} = \eta_0[1 - \beta_0(T_{cell} - 298)] \quad (12)$$

where, η_0 is the efficiency of PV cell at 25 °C and β_0 is the temperature coefficient for the cell. Consequently, the total power output from the hybrid system can be calculated using

$$P_{tot} = P_{PV} + P_{TE} \quad (13)$$

It is to be noted that the use of Eq. (13) implies a hybrid system with passive water-cooling, such as thermosiphon. If an active water-cooling system is used, the power consumption of the cooling system should be included in Eq. (13).

The overall efficiency of the hybrid system can be calculated using

$$\eta_{tot} = \eta_{PV} + \eta_{TE}\frac{1}{1 + \left(\frac{Q_c + Q_r + P_{PV}}{Q_k}\right)} \quad (14)$$

Employing appropriate operating parameters for the hybrid PV/ TEG system shown in Fig. 1, the temperature of the PV cell and the

temperature difference across the TEG can be calculated using an iterative method based on Eq. (1)–(8). The power output and conversion efficiency of the system can be determined using Eq. (9)–(14). Consequently, the optimal geometry of the TEG can be achieved by investigating the dependence of the efficiency on the geometrical factors.

3. Simulation procedure and input parameters

Simulation was performed to demonstrate the capability of the model for optimal design of hybrid PV/TEG system. A total of 8 types of TEG modules were chosen to study the dependence of the maximum power output on the geometry of TEG modules. Each type of the module has the same number of N and A_{TE}, but the length of the thermoelements was varied to obtain the maximum power output (P_{max}). The number of thermoelements (N) and the cross sectional areas (A_{TE}) employed in these modules are shown in Table 1.

The simulation uses a Matlab program to determine T_{cell} by solving Eqs. (1) and (8) iteratively. Once T_{cell} is determined, the P_{TE} and η_{TE} in closed-circuit condition can be calculated using Eqs. (9) and (10), respectively. The power output P_{PV} and efficiency η_{PV} of the solar cell are calculated using Eqs. (11) and (12), respectively. Finally, the total power output P_{tot} and conversion efficiency η_{tot} of the hybrid system can be determined using Eqs. (13) and (14), respectively. The parameters employed for the calculation are given in Table 2. The assumptions used are as follows:

1) The cold side of the thermoelectric generator is maintained constant at room temperature (298 K);
2) The intensity of solar radiation is maintained at 1000 W m^{-2}, equivalent to 1 sun of radiation flux;
3) Heat transfer occurs in one dimension only, i.e., there is no heat transfer in lateral direction;
4) The conversion efficiency of PV cell is 10% at 25 °C and changes with temperature following Eq. (12) with the temperature coefficient listed in Table 2.

The simulations were carried out in two different atmospheres: the ambient and the vacuum. The validity of the model was tested against an established theoretical procedure [25]. The calculation was carried out using type I module listed in Table 1 for an ideal operating condition where all heat losses are neglected. The results are identical for both procedures, indicating the validity of essential part of the model. Further validation to include various heat losses is being carried out against COMSOL simulation showing a good agreement (to be published elsewhere).

4. Results and discussion

Fig. 2 shows the P_{TE} as a function of l_{TE} for modules with different sizes as described in Table 1. The results were obtained for

Table 1
Geometric parameters of the modules investigated.

Module type	N	A_{TE} [mm^2]
I	62	0.64
II	62	1.44
III	62	1.96
IV	62	2.56
V	100	2.56
VI	150	2.56
VII	200	2.56
VIII	250	2.56

Table 2
Parameters used for simulation.

Parameter	Value	Unit	Reference
τ_g	0.95	–	[22]
a_c	1	–	
β_c	1	–	
β_0	0.0011	%/K	[28]
a_T	0.5	–	[22]
A_{PV}	40 × 40	mm2	
h_{cov}	5	Wm^{-2}K^{-1}	[23]
T_{amb}	298.15	K	
ε	0.88	–	[22]
k	1.5	W.m^{-1}K^{-1}	[29]
k_g	1	W.m^{-1}K^{-1}	[21]
α	185	μVK^{-1}	[29]
ρ	1×10^{-5}	Ω.m	[29]
n	0.0001	m	[30]
r	0.2	–	[30]
l_c	0.00009	m	
L_g	0.003	m	[21]

operation in atmosphere (i.e., non-vacuum). It can be seen that the P_{TE} for a given type of module increases initially with an increase in l_{TE} until reaching the P_{max} at an optimal length and then the P_{TE} starts to decrease with a further increase in l_{TE}. The results show clearly that it is necessary to design a thermoelectric module with the optimal length in order to obtain the P_{max}. It can also be seen that the P_{max} is higher for the modules that have larger N and A_{TE}. However, the optimal length required for the modules with larger N and A_{TE} is longer. This indicates that an increase in the power output is obtained at an expense of material consumption. For example, the optimal length for type VIII is 50 mm, compared with 3.4 mm for type I (i.e., a factor of 14), while the P_{max} is only increased from 5.2 mW to 7 mW. Clearly, the drawback of using longer length will overwhelm the benefit. An appropriate selection of thermoelectric module for a PV/TE system requires a compromise between the power output and material consumption. In general, the modules with small cross-sectional area are more appropriate.

It is to be noted that type VIII modules exhibit a significant increase in the P_{max} due to two reasons: 1) the semiconductor area has increased (i.e., A_{TE} in Eqs. (9) and (2)) the area of TEG becomes close to the size of PV cell and this covers all back side area of PV.
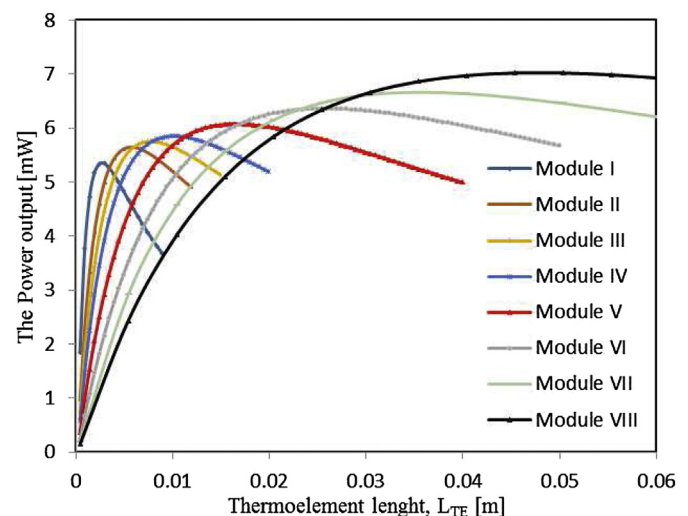

Fig. 2. Power output vs thermoelement length for system operating at ambient atmosphere.
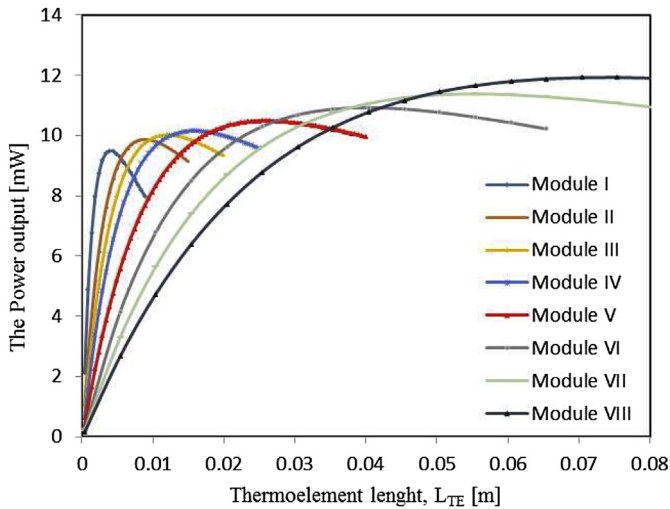
Fig. 3. Power output vs thermoelement length for system operating in vacuum.

Consequently, the heat losses by convection and radiation from the bottom side of PV cell were eliminated. This analysis indicates that the operation of PV/TE unit in vacuum can minimise the heat losses due to convection and consequently the power output is anticipated to be higher. Fig. 3 shows the P_{TE} as a function of l_{TE}, when operating in vacuum. The operation in vacuum is beneficial due to elimination of the convective losses from both sides of PV cell. It can be seen that the maximum power output of type I is almost doubled in vacuum compared with that in ambient. An increase in the power output of the smallest module (module I) when operating in vacuum is slightly more significant than that of largest module (type VIII). This can be attributed to the fact that the increase in temperature difference across the module is more significant for type I than for type VIII. It can be seen that the data in Figs. 2 and 3 are plotted as a function of thermoelement length, providing direct information on length optimisation. However, it is to be noted that the information about optimisation of other geometrical parameters such as the cross-sectional area, thermocouple number and the volume of thermoelectric materials is also embedded in these figures.

The P_{max} for each type of module as a function of volume is shown in Fig. 4 for operation in vacuum and at ambient pressure. It
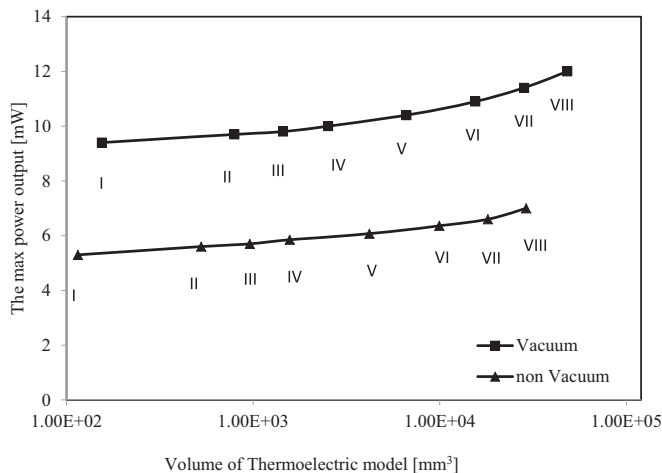
can be seen that the P_{max} of the TEG when operates in vacuum is higher than that in ambient. Increasing the volume of thermoelectric materials can improve the power output of the TEG, but the increase is very small. For example, the P_{TE} for type I is 5.2 mW and it increases to 7.0 mW for type VIII (i.e., an increase by 35%), compared with large increase in volume by more than 800%.

Fig. 5 shows the temperature difference as a function of l_{TE} for type I (smallest module) and type VIII (largest module) in vacuum and at ambient atmosphere, respectively. It can be seen that the temperature difference across a module of type I is increased by 54.8% when operating in vacuum due to elimination of the convection losses from both side of PV cell. However, the increase for type VIII is marginal if the length of thermoelements is shorter than 20 mm. Fig. 6 shows the power output per unit area as a function of l_{TE} for type I and type VIII in vacuum and at ambient atmosphere, respectively. It is apparent that the small module (type I) exhibits a significantly higher power output per unit area than that of the large module (type VIII). It is to be noted that the optimal length for achieving high power output per unit area when operated in
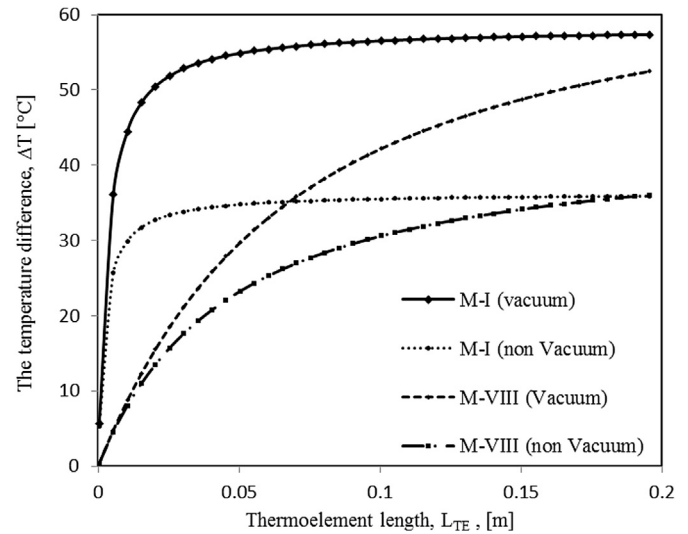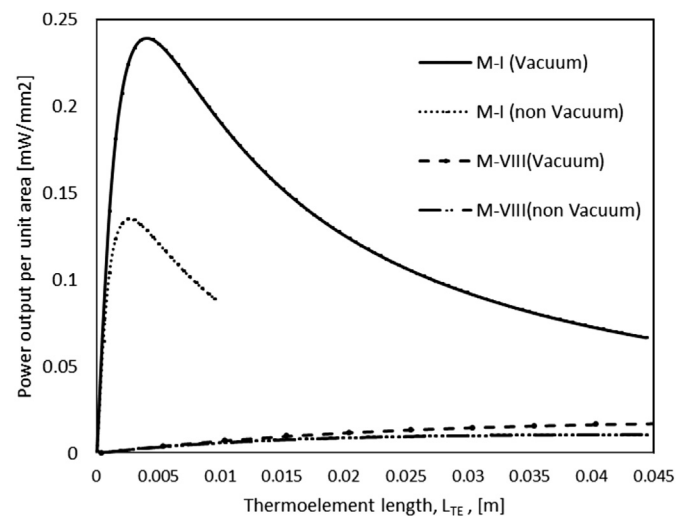

Fig. 5. Temperature difference across a module for type I and type VIII in vacuum and at ambient atmosphere, respectively.

Fig. 4. Maximum power output vs thermoelectric generator volume for operation in vacuum and at ambient atmosphere.

Fig. 6. Power output per unit area vs thermoelement length in vacuum and at ambient atmosphere, respectively.
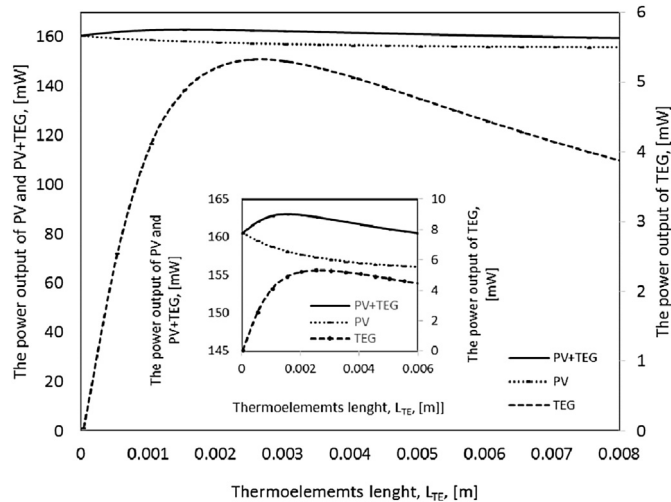
Fig. 7. The power output of TEG, PV and PV + TEG type I vs thermoelement length in ambient atmosphere.

vacuum is longer than that when operated at ambient atmosphere.

Fig. 7 shows the P_{TE}, P_{PV} and P_{tot} of type I when operating in ambient atmosphere. It can be seen that the power output of the solar cell will decrease when integrated with a TEG because the operating temperature of the solar cell is increased duo to a large thermal resistance across the TEG. However, the power reduction in the solar cell (2 mW) will be compensated by the power generation by TEG (5.2 mW). As a result, the total power output P_{tot} of the hybrid system is increased to 163 mW. Similarly, Fig. 8 shows the efficiencies η_{TE}, η_{PV} and η_{tot} of type I for operation in ambient atmosphere. For a solar cell with a cross-sectional area of 40 mm^2, the η_{tot} will increase from 10% to 10.2% for a TEG with the optimal length l_{TE} of 2 mm. A further increase in η_{tot} is possible if the system is operated in vacuum. Moreover, it has been observed that the dye-sensitised solar cells exhibit an increase in power output and efficiency with increasing temperature in a temperature range between 300 K and 340 K. This will lead to an increase in η_{PV} which will be further enhanced by η_{TE} from the thermoelectric system. Consequently, a higher increase in total efficiency is anticipated in a hybrid system with dye-sensitised solar cells [31].
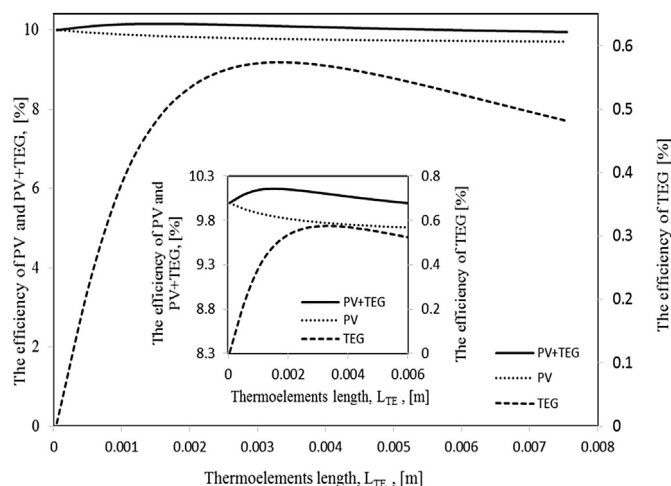

Fig. 8. The conversion efficiency of TEG, PV and PV + TEG type I vs thermoelement length in ambient atmosphere.

5. Conclusions

The optimal geometry for obtaining maximum power output and conversion efficiency of a thermoelectric generator of hybrid PV/TE system was investigated using a model developed in this paper. Together with the knowledge of temperature dependence of solar cells, the overall power output P_{tot} and conversion efficiency η_{tot} of a hybrid PV/TE system can be estimated. The results of simulation using this model shows that an increase in both the overall power output and conversion efficiency may be achieved by incorporating thermoelectric generator to harvest waste heat from photovoltaic cell. In addition, the results demonstrate that in practice an optimised geometry has to be a "trade-off" between achieving a large power output and using minimal thermoelectric material. In general, a thermoelectric module that has a smaller cross-sectional area than that of the PV cell can generate more electrical power than these of having a larger cross-sectional area. Furthermore, a significant increase in the power output can be obtained if the system operates in vacuum. In an ideal case where the convective heat losses are completely eliminate, the power output can be almost doubled.

References

[1] A. Makki, S. Omer, H. Sabir, Advancements in hybrid photovoltaic systems for enhanced solar cells performance, Renew. Sustain. Energy Rev. 41 (Jan. 2015) 658–684.
[2] M. Li, G.L. Li, X. Ji, F. Yin, L. Xu, The performance analysis of the trough concentrating solar photovoltaic/thermal system, Energy Convers. Manag. 52 (6) (Jun. 2011) 2378–2383.
[3] M. Li, X. Ji, G.L. Li, Z.M. Yang, S.X. Wei, L.L. Wang, Performance investigation and optimization of the trough concentrating photovoltaic/thermal system, Sol. Energy 85 (5) (May 2011) 1028–1034.
[4] B. Huang, T. Lin, W. Hung, F. Sun, Performance evaluation of solar photovoltaic/thermal systems, Sol. Energy 70 (5) (Jan. 2001) 443–448.
[5] T.T. Chow, W. He, J. Ji, Hybrid photovoltaic-thermosyphon water heating system for residential application, Sol. Energy 80 (3) (Mar. 2006) 298–306.
[6] T.T. Chow, W. He, J. Ji, A.L.S. Chan, Performance evaluation of photovoltaic–thermosyphon system for subtropical climate application, Sol. Energy 81 (1) (Jan. 2007) 123–130.
[7] T.T. Chow, G. Pei, K.F. Fong, Z. Lin, A.L.S. Chan, J. Ji, Energy and exergy analysis of photovoltaic–thermal collector with and without glass cover, Appl. Energy 86 (3) (Mar. 2009) 310–316.
[8] D. Yang, H. Yin, Energy conversion efficiency of a novel hybrid solar system for photovoltaic, thermoelectric, and heat utilization, IEEE Trans. Energy Convers. 26 (2) (Jun. 2011) 662–670.
[9] E.A. Chávez-Urbiola, Y.V. Vorobiev, L.P. Bulat, Solar hybrid systems with thermoelectric generators, Sol. Energy 86 (1) (Jan. 2012) 369–378.
[10] Y. Vorobiev, J. González-Hernández, P. Vorobiev, L. Bulat, Thermal-photovoltaic solar hybrid system for efficient solar energy conversion, Sol. Energy 80 (2) (Feb. 2006) 170–176.
[11] H. Hashim, G. Min, Investigate the maximum power output from solar cells for integration with thermoelectric generator in a hybrid solar energy system, in: International Conference on Solar Energy for MENA Region (INCOSOL), Amman, 2012, pp. 22–23.
[12] Y.-Y. Wu, S.-Y. Wu, L. Xiao, Performance analysis of photovoltaic–thermoelectric hybrid system with and without glass cover, Energy Convers. Manag. 93 (Mar. 2015) 151–159.
[13] B.S. Dallan, J. Schumann, F.J. Lesage, Performance evaluation of a photoelectric–thermoelectric cogeneration hybrid system, Sol. Energy 118 (Aug. 2015) 276–285.
[14] Hashim Hasan, G. Min, Enhance the performance of hybrid dye sensitised solar cell/thermoelectric system, in: Photovoltaic Science Applications and Technology, PVSAT-9, 2013, pp. 141–144.
[15] H. Chang, Z.-R. Yu, Integration of dye-sensitized solar cells, thermoelectric modules and electrical storage loop system to constitute a novel photothermoelectric generator, J. Nanosci. Nanotechnol. 12 (8) (Aug. 2012)

6811—6816.

[16] H. Chang, M.-J. Kao, K.-C. Cho, S.-L. Chen, K.-H. Chu, C.-C. Chen, Integration of CuO thin films and dye-sensitized solar cells for thermoelectric generators, Curr. Appl. Phys. 11 (4) (Jul. 2011) S19—S22.

[17] H. Chang, M.-J. Kao, K.D. Huang, S.-L. Chen, Z.-R. Yu, A novel photo-thermoelectric generator integrating dye-sensitized solar cells with thermo-electric modules, Jpn. J. Appl. Phys. 49 (6) (Jun. 2010) 06GG08.

[18] Y. Zhang, J. Fang, C. He, H. Yan, Z. Wei, Y. Li, Integrated energy-harvesting system by combining the advantages of polymer solar cells and thermoelec-tric devices, J. Phys. Chem. C 117 (47) (Nov. 2013) 24685—24691.

[19] B. Agrawal, G.N. Tiwari, Optimizing the energy and exergy of building inte-grated photovoltaic thermal (BIPVT) systems under cold climatic conditions, Appl. Energy 87 (2) (Feb. 2010) 417—426.

[20] A.S. Joshi, A. Tiwari, Energy and exergy efficiencies of a hybrid photo-voltaic—thermal (PV/T) air collector, Renew. Energy 32 (13) (Oct. 2007) 2223—2241.

[21] F. Sarhaddi, S. Farahat, H. Ajam, a. Behzadmehr, Exergetic performance assessment of a solar photovoltaic thermal (PV/T) air collector, Energy Build. 42 (11) (Nov. 2010) 2184—2199.

[22] H. Najafi, K.a Woodbury, Modeling and analysis of a combined photovoltaic-thermoelectric power generation system, J. Sol. Energy Eng. 135 (3) (Apr. 2013) 031013.

[23] X. Ju, Z. Wang, G. Flamant, P. Li, W. Zhao, Numerical analysis and optimization of a spectrum splitting concentration photovoltaic—thermoelectric hybrid system, Sol. Energy 86 (6) (Jun. 2012) 1941—1954.

[24] G. Min, ZT measurements under large temperature differences, J. Electron. Mater 39 (9) (Mar. 2010) 1782—1785.

[25] G. Min, Thermoelectric module design under a given thermal input: theory and example, J. Electron. Mater 42 (7) (2013) 2239—2242.

[26] G. Min, TE module design theories, in: D.M. Rowe (Ed.), CRC Handbook of Thermoelectrics: Micro to Nano, CRC Press, Boca Ration, 2006, pp. 11.1—11.15.

[27] D.L. Evans, Simplified method for predicting photovoltaic array output, Sol. Energy 27 (6) (1981) 555—560.

[28] RETScreen International, Photovoltaic Project Analysis, 2001, p. 22.

[29] D.M. Rowe, CRC Handbook of Thermoelectrics, London CRC Press, London, 1996.

[30] D.M. Rowe, G. Min, Evaluation of thermoelectric modules for power genera-tion, J. Power Sources 73 (2) (1998) 193—198.

[31] S.R. Raga, F. Fabregat-Santiago, Temperature effects in dye-sensitized solar cells, Phys. Chem. Chem. Phys. 15 (7) (Feb. 2013) 2328—2336.